SSRG International Journal of Civil Engineering
ISSN: 2348-8352/ https://doi.org/10.14445/23488352/IJCE-V11I6P108

Volume 11 Issue 6, 60-70, June 2024

Original Article

Confinement Behaviour of Ferrogeopolymer Brick Masonry Columns: Experimental and Theoretical Analysis

R. Jose Antony Syril[1], D. Rajkumar[2]

[1,2]*Department of Civil and Structural Engineering, Annamalai University, Tamilnadu, India.*

[1]*Corresponding Author : joseantonysyrilr@gmail.com*

Received: 11 April 2024 Revised: 22 May 2024 Accepted: 10 June 2024 Published: 30 June 2024

Abstract - *This study investigates the confinement behaviour of ferrogeopolymer brick masonry columns using experimental testing and theoretical analysis. The objective is to assess failure modes and stress-strain behaviour and compare experimental findings with theoretical predictions. The experiments involve subjecting brick masonry columns to axial loads and confining them using different surface coatings and additional reinforcement layers. The results show significant disparities in the accuracy of confinement ratio prediction between the Indian Standard 1905-1987 and Cascardi et al.2017 models. The Cascardi model demonstrates superior accuracy and is better suited for predicting the confinement behaviour of masonry specimens under axial compression. This research advances computational procedures, enhances our understanding of the behaviour of ferrogeopolymer brick masonry columns, and ensures their safety and stability in various structural applications.*

Keywords - *Ferrogeopolymer, Brick masonry columns, Steel mesh, Confinement, Theoretical analysis.*

1. Introduction

Brick masonry is a construction technique used for various structures, such as walls, columns, arches, and facades [1]. Bricks, made from clay or concrete, are chosen for their durability, strength, and aesthetics. However, traditional brick masonry has limitations in terms of seismic resistance and structural performance. During earthquakes or lateral loading events, masonry columns can deform and fail [2]. To address this vulnerability, engineers have developed techniques to confine masonry columns, including the use of ferrocement with steel mesh. Ferrocement is a composite material of cement mortar reinforced with layers of steel mesh or fibres [3-5]. It prevents outward deformation, enhances load-carrying capacity, improves ductility, and enhances overall structural performance. This increases resistance to earthquakes and wind. Additionally, ferrocement adheres strongly to the masonry surface, ensuring a durable bond. Over the past few years, there has been interest in alternative construction materials that offer sustainability and high performance, such as geopolymer and ferrogeopolymer. Geopolymer is an inorganic polymer composite created from natural substances like fly ash, slag, or metakaolin combined with alkaline activators [6-8]. These materials undergo a chemical reaction to form a durable structure. In geopolymer production, the raw materials are mixed with alkaline activators like sodium hydroxide or potassium hydroxide to create a paste. This paste is poured into moulds and allowed to cure and harden at ambient temperature. Geopolymer has advantages over traditional Portland cement, including environmental sustainability, high strength, corrosion and fire resistance, and reduced shrinkage and creep [9]. Ferrogeopolymer is a variation of geopolymer that incorporates steel fibres or mesh reinforcement within the geopolymer matrix. This results in a composite material with enhanced mechanical properties, including improved tensile strength, ductility, and durability. Ferrogeopolymer offers sustainable and high-performance alternatives to conventional construction materials [10, 11]. The manufacturing process for ferrogeopolymer is similar to that of geopolymer, with the addition of steel reinforcement. Steel fibres or mesh are added to the geopolymer paste before casting, creating a composite material with superior structural performance. Ferrogeopolymer combines the advantages of geopolymer with the benefits of steel reinforcement, such as increased load-carrying capacity and improved structural performance. Various researchers have conducted studies on brick masonry confinement and ferrogeopolymer construction methods. Sneha et al. (2020) [12] examined the mechanical properties and corrosion resistance of different ferrocement systems, highlighting the superior flexural strength of welded mesh specimens. Corrosion prevention methods, such as corrosion inhibitors and CPC coatings, were found to improve durability and load capacity effectively. Joseph Davidovits (1994) [13] emphasized the cost-effectiveness and environmental

advantages of geopolymer cement compared to traditional Portland cement, emphasizing their potential for sustainable infrastructure development. Rajendran and Soundarapandian (2013, 2014, 2015) [14-16] investigated the influence of increased molarity on the flexural load performance and compressive strength of geopolymer ferrocement slabs, observing positive effects. Hasan (2022) [17] examined the fortification of brick masonry columns with ferrocement and reinforced concrete jacketing, noting significant enhancements in strength and ductility. Sen et al. (2023) [18] studied the lateral strength of reinforced concrete frames with ferrocement-strengthened masonry infills, proposing theoretical computation procedures for various failure mechanisms.

Reinhorn et al. (1985) [19] conducted experiments with thin ferrocement overlays as seismic retrofit materials for masonry walls, demonstrating strength, ductility, and stiffness improvements. Faella et al. (2011) [20] aimed to develop accurate design formulas for Fibre-Reinforced Polymer (FRP)-confined masonry columns, presenting three design formulas of varying levels of accuracy and complexity that can be used in practical applications. Comprehensive guidelines for designing masonry structures to ensure their safety, durability, and serviceability are provided by Eurocode 6 - EN1996-1-1 [21] and IS 1905-1987 [22]. Cascardi et al. (2017) [23] investigated the compressive strength of columns confined by Fiber Reinforced Mortar (FRM) and proposed new design models that considered both fibre and matrix properties.

These models demonstrated high predictive capability and accuracy for implementation. Theoretical analysis plays a crucial role in optimising confinement techniques for brick masonry columns. Engineers utilise mathematical modelling and simulation to understand column behaviour under different loading conditions, facilitating improved performance and safety. Theoretical analysis of confinement techniques using ferrocement with steel mesh, geopolymer, or ferrogeopolymer involves evaluating material properties, column dimensions, loading conditions, and optimisation.

The literature review has identified a novel research gap in the confinement of masonry columns, ferrocement, and geopolymer ferrocement, as well as the need for validated computation procedures for assessing the load-carrying capacity of brick masonry columns. While lateral strength studies exist, validated theoretical models for ferrocement-strengthened masonry columns are lacking. Developing and validating procedures to predict load-carrying capacity under axial loads is necessary, ensuring accuracy by comparing theoretical predictions with experimental data. This research will enhance understanding and ensure the safety and stability of ferrocement-strengthened masonry columns in various applications. This study introduces a novel approach by evaluating failure modes stress-strain behavior and comparing experimental and theoretical results in brick masonry columns with different surface coatings (cement mortar and geopolymer mortar) and reinforcement layers (single-layer and double-layer welded steel mesh). The unique combination of coatings and reinforcement layers, particularly the use of geopolymer mortar and the comparison of single versus double layers, offers new insights and could lead to improved construction techniques and safety measures for masonry structures.

2. Materials and Methods

Table 1 presents the details of the specimens utilized for analysing the influence of confinement on masonry columns under concentric axial load. These specimens are categorized into three series: unconfined, conventionally confined, and geopolymer confined. Each sample is assigned a designation of A-B, where A denotes the type of mortar and B indicates the number of steel mesh layers used for confinement.

The geometric characteristics of the masonry columns are shown in Figure 1. Previously, an experimental investigation was carried out on steel meshed Cement Mortar (CM) and Geopolymer Mortar (GPM) confined masonry columns. A comprehensive description of this investigation can be found in a separate paper. The comparative analysis of the test results, which will be discussed in the subsequent sections, encompasses all of the confined specimens that were subjected to testing.

Table 1. Details of tested specimens

Series	Sample ID	No. of Layers	Sample Description
Conventional	UC	-	A specimen without additional confinement material
Conventional Confined	CC-0	-	Cement mortar surface coating
	CC-1	1	Cement mortar with welded mesh single-layer
	CC-2	2	Cement mortar with welded mesh Double-layer
Geopolymer Confined	GP-0	-	Geopolymer mortar surface coating
	GP-1	1	Geopolymer mortar with welded mesh single-layer
	GP-2	2	Geopolymer mortar with welded mesh Double-layer

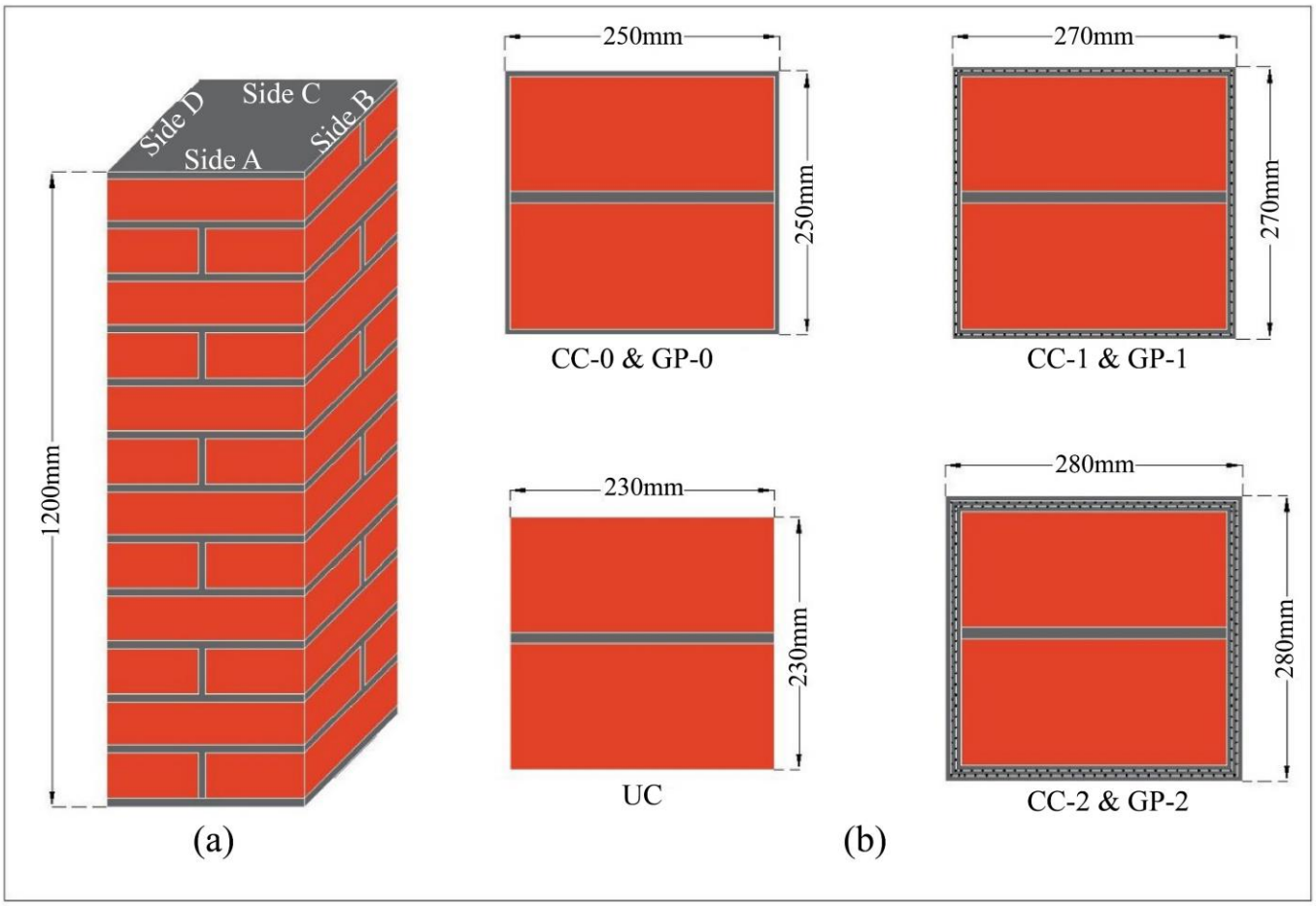

Fig. 1 Geometry of the masonry column (a) Elevation, and (b) Cross section.

2.1. Clay Burnt Bricks and Binding Mortar

According to the Indian standard (IS 1077-1992) [24], non-modular clay-burnt bricks measuring 230mm x 110mm x 70mm were used for constructing brick masonry columns. These bricks had a density of 1569 kg/m^3 and a water absorption rate of 16.12%. In this study, two types of mortars were used: CM and GPM. The mortar mix ratio for CM was 1:2 (binder to fine aggregate), and for GPM, it was 1:2.5. The geopolymer mortar consisted of fly ash, Sodium Silicates (Na_2SiO_3), Sodium Hydroxide (NaOH), and Naphthalene Sulfonate-based Superplasticizer (SP), and distilled water, for the preparation of GPM, a sodium hydroxide concentration of 8 molarity was chosen. Mortar cubes measuring 70.6 mm × 70.6 mm × 70.6 mm were cast, following the guidelines of IS 4031 (Part-6) - 1988 [25], to test the characteristic strength of the mortar mix. Table 2 displays the compressive strength of both mortar cubes and bricks. The values presented in the table represent the average compressive strength of ten specimens for both bricks and mortar.

Table 2. Compressive strength of brick and mortar

Description	Brick	CM	GPM
Compressive Strength (MPa)	5.31	14.93	21.6

2.2. Welded Steel Mesh

The machine-welded mesh used in this study has square openings measuring 20mm × 20mm and a thickness of 0.75mm. To evaluate its mechanical properties, three specimens were subjected to tensile tests according to the ASTM A 185 standard [26]. Figure 2 displays the stress-strain graph, and Table 3 provides the mechanical properties obtained from the tests.

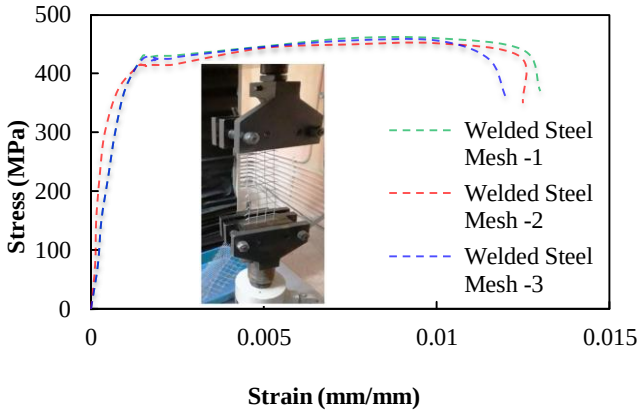

Fig. 2 Stress-Strain for welded steel mesh

Table 3. Mechanical properties welded steel mesh

Sample	Yield Tensile Stress (MPa)	Ultimate Tensile Stress (MPa)	Elastic Modulus (MPa)	Ultimate Strain (mm/mm)
1	421	456	136320	0.012
2	418	452	134522	0.0125
3	424	460	138148	0.013
Mean	421	456	136330	0.0125

2.3. Specimen Preparation

A total of fourteen specimens were prepared for this experiment. Each combination consisted of two specimens, resulting in seven combinations in total. The preparation process involved mixing mortar according to the prescribed mix ratio, constructing masonry columns using clay-burnt bricks, and applying surface coatings as necessary. To enhance confinement, welded wire mesh reinforcement was installed in all specimens except for the unconfined ones. The conventional specimens underwent water curing, while the geopolymer specimens were left to cure under ambient conditions. Once cured, the specimens were whitewashed, marked for dimensional accuracy, and transported to the test floor for axial compression testing. Figure 3 provides a visual representation of how the specimens were prepared for the experiment

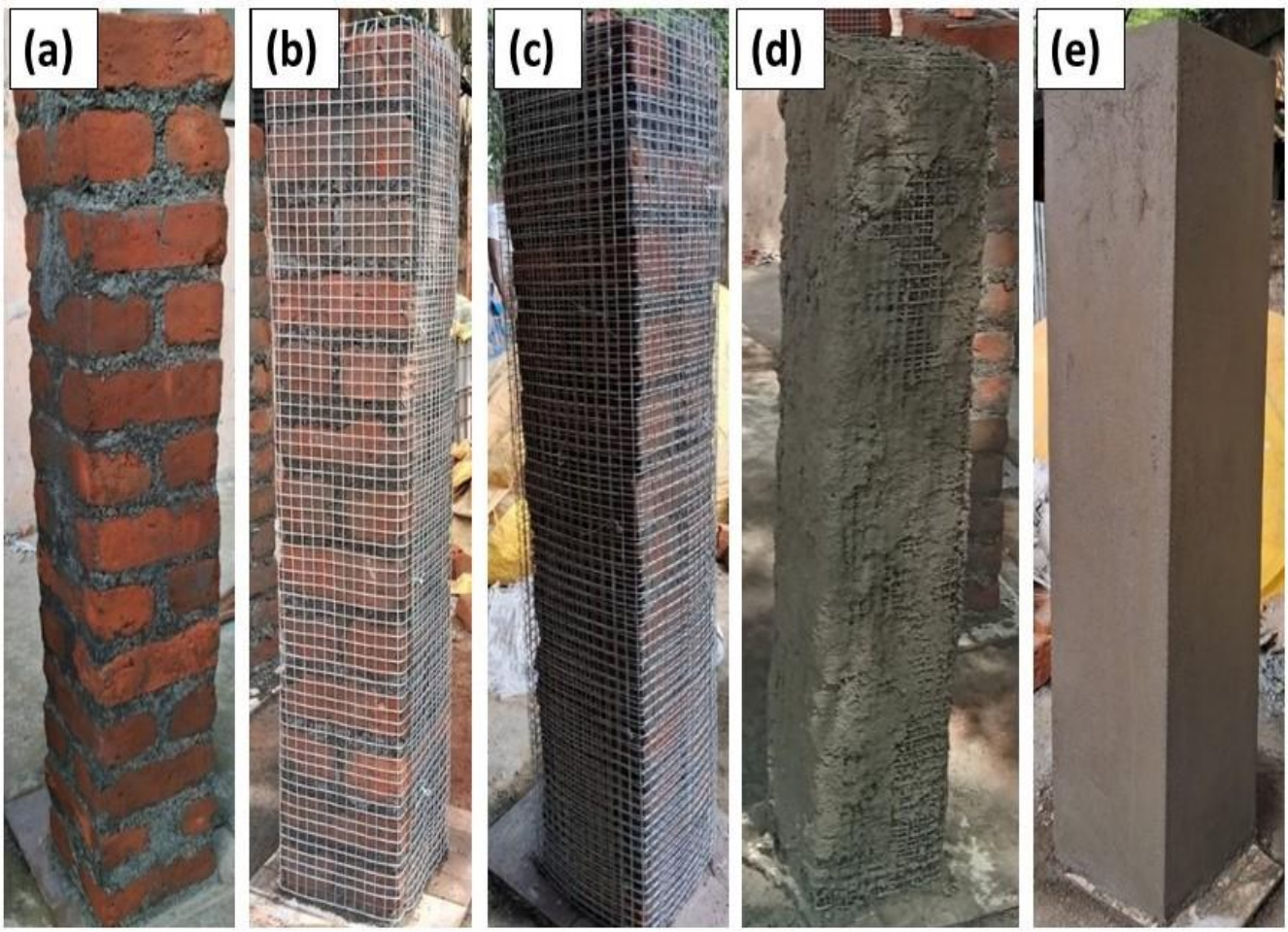

Fig. 3 Preparation of Specimens (a) Unconfined, (b) Single layer, (c) Double layer, (d) Applying surface coating, and (e) Surface finished.

2.4. Test Setup

The experimental configuration and schematic setup shown in Figure 4 utilize a hydraulic testing machine with a maximum capacity of 500 kN to perform tests on column specimens.

This setup ensures that there is enough capacity to apply axial compression loads to the masonry column specimens. Each specimen is equipped with a 20mm thick steel plate cap on both the top and bottom, which serves to evenly distribute the load from the hydraulic testing machine across the top surface of the specimen. The load is applied incrementally at intervals of approximately 2.5 kN until failure occurs.

To measure displacement, four Linear Variable Differential Transformers (LVDTs) are positioned horizontally on each side of the specimen, while one LVDT is placed vertically to monitor vertical displacement.

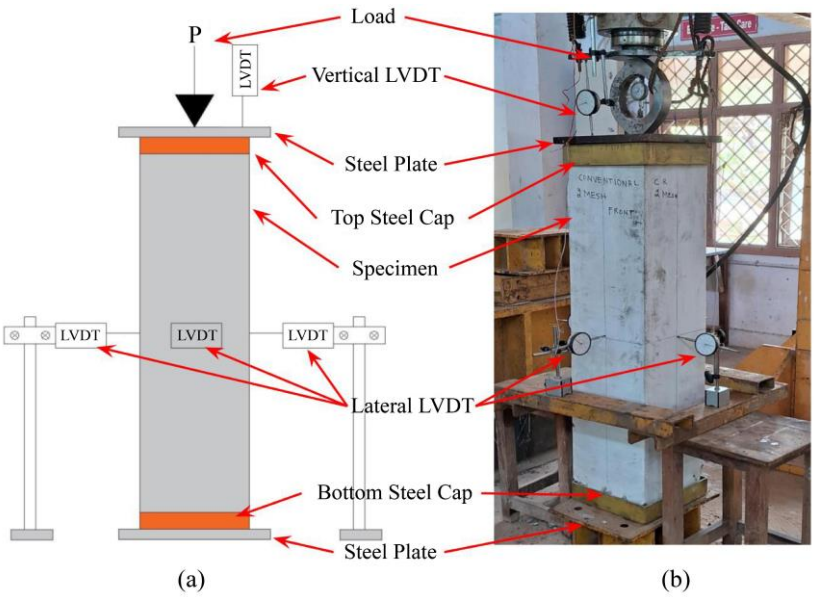

Fig. 4 Test setup (a) Schematic, and (b) Experimental.

3. Results and Discussion

3.1. Failure Modes

Figure 5 presents a depiction of the various failure configurations observed in the tested specimens. These failures predominantly involve masonry crushing, detachment of the external mortar layer, and separation of the steel wire mesh from both the masonry and mortar. For instance, Unconfined Specimens (UC) fail primarily due to masonry crushing, typically accompanied by the development of a wide vertical crack in the centre of the specimens. This phenomenon is particularly prominent in specimens lacking steel mesh reinforcement (CC-0 and GP-0). Confined specimens, on the other hand, exhibit different failure modes depending on the level of confinement. Specimens with single and double layers of confinement (CC-1, CC-2, GP-1, and GP-2) demonstrate "knife effects," characterized by the generation of corner cracks originating from the corners of the column. These cracks indicate localized failure and detachment of the surface-coated mortar. Consequently, the wire mesh reinforcement and surface-coated mortar become detached, signifying significant structural distress and loss of integrity.

3.2. Ultimate Load and Stress-Strain Behaviour

Table 4 presents the ultimate load values for all tested specimens. The results indicate that the confinement ratio (ξ) - which compares the ultimate load of confined columns to the ultimate load of unconfined specimens - is affected by the number of confining layers. For conventional specimens, ξ ranges from 1.54 to 3.85, with an increase as the number of confining layers increases. The same trend can be observed for geopolymer columns, with ξ values of 1.77 and 5.69, respectively. Comparing the ultimate load values of CC-0 and GP-0 specimens - both coated with cement mortar and geopolymer mortar - highlights the impact of mortar configuration on the ultimate load. The ultimate load of the GP-0 specimen is 15% higher than that of the CC-0 specimen. Further analysis of the results reveals that both CC-1 and GP-1 columns are confined with a single layer of welded steel mesh, emphasizing the influence of the steel mesh in combination with geopolymer mortar. GP-1 exhibits a 74% higher ultimate load than CC-1. Similarly, CC-2 and GP-2, with double layers, demonstrate an increased load-carrying capacity, with GP-2 being 48% higher than CC-2.

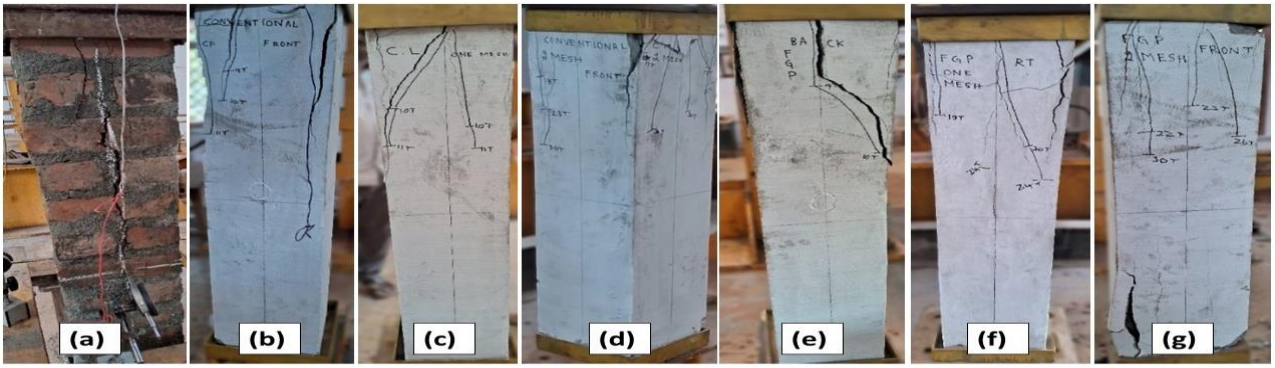

Fig. 5 Failure of specimens (a) UC, (b) CC-0, (c) CC-1, (d) CC-2, (e) GP-0, (f) GP-1, and (g) GP-2.

Table 4. Experimental test results at the ultimate condition

Specimen ID	Axial Load (kN)	Confinement Ratio, ξ	Axial Stress (MPa)	Axial Strain (ε_a) (mm/mm)	Lateral Strain (ε_l) (mm/mm)
UC	65	-	1.23	0.0021	0.0044
CC-0	100	1.54	1.60	0.0015	0.0038
CC-1	115	1.77	1.58	0.0041	0.0035
CC-2	250	3.85	3.19	0.0058	0.0073
GP-0	115	1.77	1.84	0.0016	0.0037
GP-1	200	3.08	2.74	0.0086	0.0129
GP-2	370	5.69	4.72	0.0134	0.0096

The stress and strain behaviours of masonry columns were determined through tests involving concentric axial loads, as shown in Figure 6 for all tested specimens. Strain values were derived from displacement measurements taken during the tests using a strain indicator. The average strain values recorded at the mid-height of the columns are presented. The stress-strain curves indicate that masonry columns exhibit elastic behaviour during the initial stage and nonlinear behaviour leading to failure.

Specimen UC exhibited limited stress-strain behaviour, indicating sudden and brittle failure due to lack of confinement. In contrast, confined specimens displayed superior stress-strain behaviour compared to the unconfined column. This can be attributed to the presence of a steel mesh layer, which resists lateral displacement and enables the column to withstand higher stress levels. The axial stress ranged from 1.23 to 4.72 MPa, axial strain ranged from 0.0015 to 0.0134, and lateral strain ranged from 0.0035 to 0.0129.

The experimental results indicate that the specimens subjected to axial compression exhibited a wide range of behaviours. Both Cement mortar (CC) and Geopolymer mortar (GP) specimens demonstrated an increase in axial stress with increasing confinement and strain. For instance, when comparing CC-0 to CC-2, there is a significant increase in axial stress and strain, highlighting the effect of the number of confinement layers.

A similar trend is observed in geopolymer mortar specimens, with GP-0 showing lower axial stress and strain compared to GP-1 and GP-2. Furthermore, lateral strain increased with increasing axial stress, indicating the dilation of the specimens under compression. This behaviour is more pronounced in geopolymer mortar specimens, particularly in GP-1 and GP-2. These findings demonstrate the complex behaviour of masonry specimens under axial compression and underscore the importance of considering factors such as material type, confinement, and strain response in structural design and analysis.

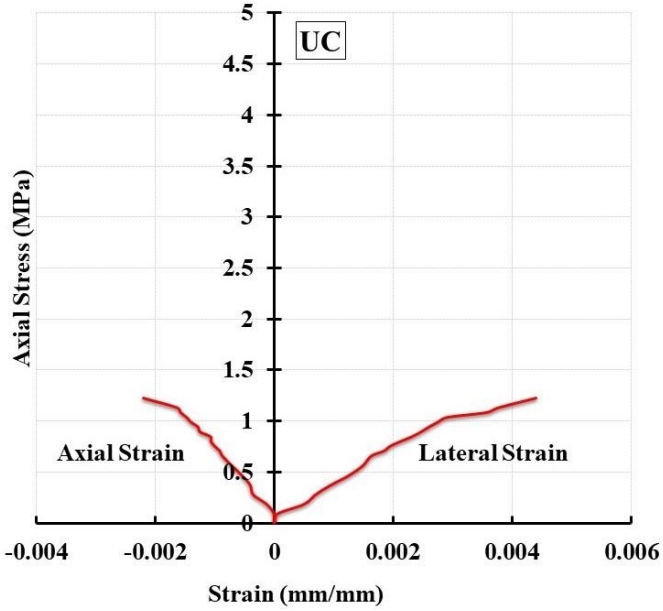

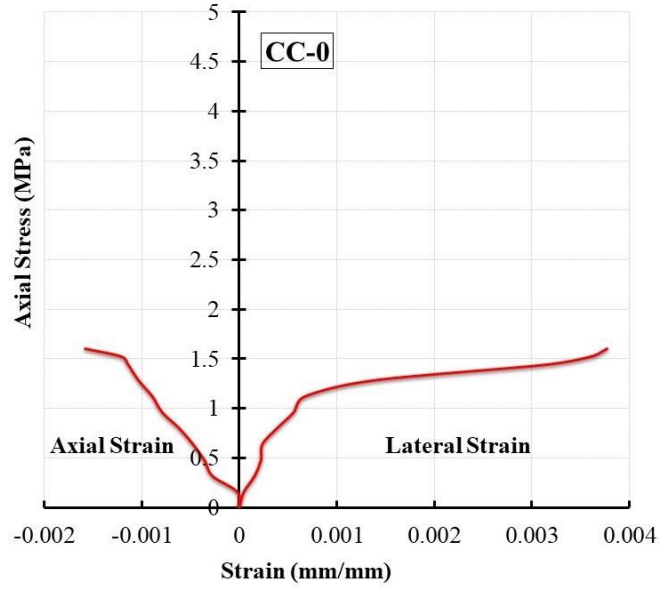

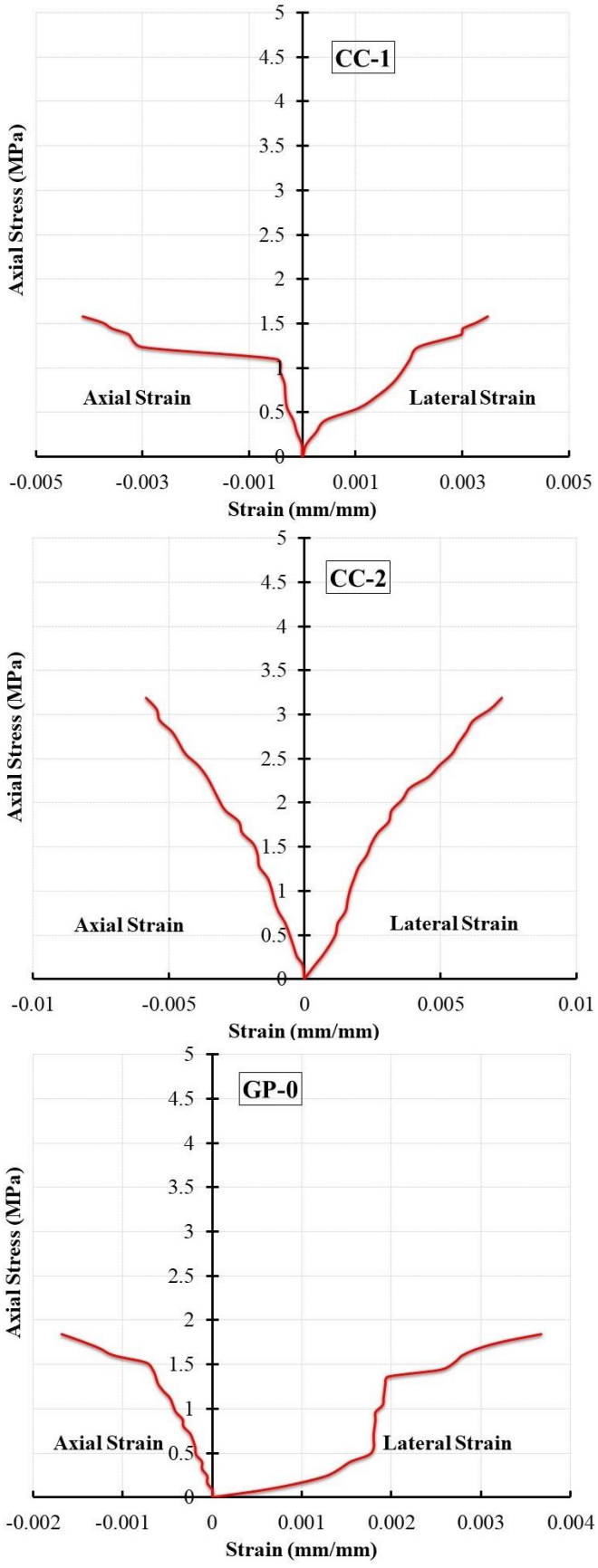

Fig. 6 Stress-strain curves

4. Experimental-Theoretical Comparison

The design of brick masonry columns follows the guidelines provided by the relevant Indian Standard IS 1905-1987 code provisions [22]. These guidelines propose a model for predicting the strength of confined masonry columns. The strength increase due to confinement can be calculated using Equation 1.

$$f_{mc} = f_m + C_e k_1 \sigma_L \quad (1)$$

Where, f_m – Compressive strength of brick masonry prism, k_1 – The strength increase factor is generally taken as 4.0, C_e – Confinement effectiveness coefficient varies with (σ_L/σ_o) ratio and can be obtained from the graph (Figure 7), σ_L – Stress of Lateral confinement, σ_o – Stress of unconfined column. The effective confinement coefficient (C_e) is a measure of the efficiency of the confinement system in

enhancing the compressive strength of masonry columns. It is crucial to understand the behaviour of confined masonry under axial loads. The C_e can also be calculated using the following formula (Equation 2).

$$C_e = \frac{f'_{mc} - f_{mc}}{f_{mc}} \quad (2)$$

Where:

f'_{mc} – is the confined compressive strength, f_{mc} – is the unconfined compressive strength.

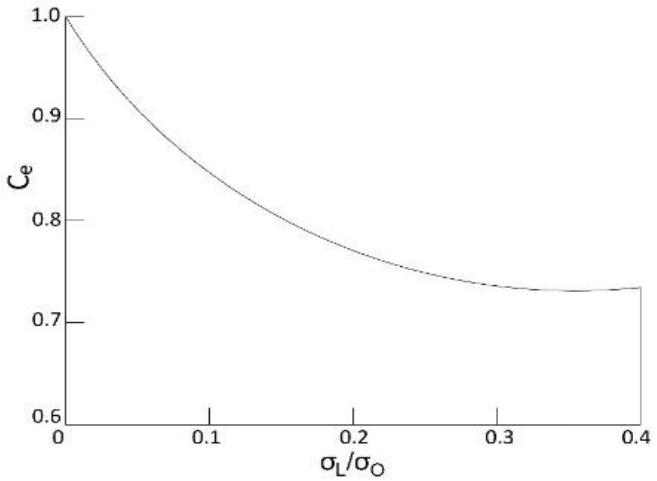

Fig. 7 Confinement effectiveness coefficient

The compressive strength of a brick masonry prism can be predicted using the formula (Equation 3).

$$f_m = \sqrt{f_b} + \sqrt[3]{f_j} \quad (3)$$

Where, f_b – Basic Compressive stress 0.25 times of f_m or compressive strength of brick, f_j – Compressive strength of mortar. The additional stress the reinforcement system applies to a masonry column is the confinement stress (σ_{con}) to enhance its load-carrying capacity, which can be calculated using Equation 4.

$$\sigma_{con} = C_e \times f_{mc} \quad (4)$$

The lateral confinement pressure using the formula (Equation 5).

$$\sigma_L = \frac{2N_{ml}W_{yl}}{(S_p - d_m)} \quad (5)$$

Where, N_{ml} – number mesh layer, W_{yl} – yield load of steel mesh, S_p – spacing of mesh, d_m – the mean distance between the outer mesh layer and the inlner mesh layer.

Furthermore, Cascardi et al. 2017 [23] have recently proposed a model that employs a multiple linear regression approach. This model specifically considers two crucial parameters: the mortar strength and the elastic modulus of the fibres. To enhance practicality, Cascardi et al. 2017 [23] also put forth a simplified version of the model, which can be mathematically expressed as follows (Equation 6):

$$\frac{f_{mc}}{f_{mo}} = 1 + k\left(\frac{f_{l,eff}}{f_{mo}}\right)^{0.5} \quad (6)$$

When considering f_{mc} and f_{mo} the compression strength of confined and unconfined columns, respectively, can be represented by $f_{l,eff}$, which is the effective confining pressure (Equation 7) expressed as a function of the maximum confinement pressure, f_l.

$$f_{l,eff} = k_H f_l \quad (7)$$

$$f_l = \frac{2n_f t_f E_f \varepsilon_f}{D} \quad (8)$$

$$k_H = 1 - \frac{(b-2r)^2 + (h-2r)^2}{3bh} \quad (9)$$

Equations (8) and (9) define n_f as the number of steel mesh layers t_f as the thickness of the steel mesh, b and h as the length and width of the column's cross-section, D as the diagonal length of the cross-section, and r as the radius of the rounding corner of the column's cross-section. The tensile strain of the steel mesh ε_f. Equation (10) expresses the coefficient k as follows:

$$k_{mat} = 6.0\,\rho_{mat}\frac{f_{mat}}{f_{mo}} \quad (10)$$

f_{mat} represents the compressive strength of the mortar and ρ_{mat} indicates the geometric percentage of mortar in the ferrocement (Equation 11).

$$\rho_{mat} = 4\frac{t_{mat}}{D} \quad (11)$$

Where t_{mat} is the thickness of the ferrocement layer.

Table 5 presents the confinement ratios obtained from Experimental testing (Exp), as well as the predictions made by the IS 1905-1987 model and the Cascardi et al. (2017) model for the tested specimens (CC-1, CC-2, GP-1, and GP-2). CC-0 and GP-0 have been excluded from the analysis due to their lack of confinement.

The experimental results demonstrate significant variations in the obtained confinement ratios for the tested specimens. Both the IS 1905-1987 and Cascardi et al. (2017) models were used to predict the confinement ratios, and the ratio of predicted to experimental (Pre/Exp) values was calculated to assess the accuracy of each model. It is important to note the average confinement ratio, as well as the corresponding standard deviation and Coefficient of Variation (CoV), for each model. The IS 1905-1987 model shows an average confinement ratio of 2.519, with a standard deviation of 0.810 and a CoV of 0.321. On the other hand, the Cascardi

et al. (2017) model exhibits an average confinement ratio of 1.355, with a standard deviation of 0.198 and a CoV of 0.146. The experimental results indicate that the actual confinement ratios vary significantly across different specimens, ranging from 1.769 to 5.692. However, both models provide predictions that deviate from the experimental values to varying degrees. For the IS 1905-1987 model, the average Pre/Exp ratio is approximately 0.924, with a standard deviation of 0.662 and a CoV of 0.715. Similarly, for Cascardi et al. (2017), the average Pre/Exp ratio is approximately 0.435, with a standard deviation of 0.154 and a CoV of 0.354. In addition to comparing the experimental confinement ratios with predictions from the IS 1905-1987 and Cascardi et al. (2017) models, a scatter plot was generated to analyze the relationship between experimentally obtained axial stress values and those predicted by the two models. The scatter plot (Figure 8) analysis reveals a strong correlation between the experimental axial stress values and the predictions from both the IS 1905-1987 and Cascardi et al. (2017) models. The coefficient of determination (R^2) was found to be 0.74 for the IS 1905-1987 model and 0.99 for the Cascardi et al. (2017). A higher R^2 value indicates a better fit of the model to the experimental data. The R^2 value of 0.99 for the Cascardi *et al.* (2017) model suggests that 99% of the variability in the experimental axial stress values can be explained by the predictions of the Cascardi et al. (2017) model, indicating its superior accuracy compared to the IS 1905-1987 model.

Table 5. Comparison of Predicted Model / Experimental

Sample ID	Confinement Ratio (Exp)	IS 1905-1987 Model	Pre/Exp	Cascardi et al. 2017 Model	Pre/Exp
CC-1	1.769	3.476	1.965	1.220	0.689
CC-2	3.846	2.071	0.539	1.361	0.354
GP-1	3.077	2.668	0.867	1.318	0.428
GP-2	5.692	1.859	0.327	1.522	0.267
Mean	2.397	2.519	0.924	1.355	0.435
Standard Deviation	3.021	0.810	0.662	0.198	0.154
Coefficient of Variation	0.840	0.321	0.715	0.146	0.354

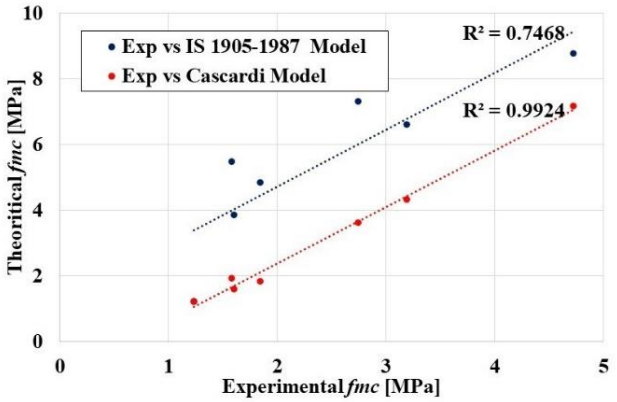

Fig. 8 Correlation between theoretical and experimental

Upon comparing the two models, it is evident that the Cascardi et al. (2017) model provides a more accurate forecast of the confinement ratio for the tested specimens. This assertion is supported by its lower average Pre/Exp ratio, standard deviation, coefficient of variation, and higher R^2 value. Consequently, we can deduce that the Cascardi et al. (2017) model is more suitable for predicting the confinement behaviour of masonry specimens under axial compression, thereby offering superior accuracy compared to the IS 1905-1987 model. To ensure the reliability and applicability of the Cascardi et al. (2017) model across a wider range of masonry materials and configurations, it is recommended to conduct further analysis and verification. Several key factors contributed to these improved results compared to state-of-the-art techniques. Firstly, the material properties of ferrogeopolymer, with its excellent compressive strength, make it an ideal candidate for structural applications, and its ability to form strong bonds with the wire mesh further enhances the confinement effect. Secondly, the welded wire mesh provides uniform and continuous confinement, preventing localized failures and ensuring a more homogeneous stress distribution. Additionally, the use of double-layer reinforcement in some specimens further improved the structural behaviour, demonstrating the effectiveness of this configuration in enhancing load resistance. The practical implications of adopting our technique in construction practices include the potential for more durable and cost-effective masonry structures. Ferrogeopolymer not only enhances structural performance but also offers environmental benefits due to its lower carbon footprint compared to traditional cement-based materials. Overall, our study provides a comprehensive analysis of the confinement behaviour of ferrogeopolymer brick masonry columns, offering significant advancements over state-of-the-art techniques and contributing to the development of more efficient and sustainable construction methods.

5. Conclusion

- Unconfined masonry specimens exhibit sudden and brittle failure due to crushing, while confined specimens with a steel mesh layer demonstrate superior behaviour. Confined specimens display "knife effects" with corner

cracks, indicating localized failure and detachment of surface-coated mortar and wire mesh reinforcement, signifying significant structural distress.

- The number of confining layers significantly influences the ultimate load of both conventional and geopolymer specimens. Comparing mortar configurations, GP-0 shows a 15% higher load than CC-0. The addition of welded steel mesh enhances load-carrying capacity, with GP-1 and GP-2 specimens showing 74% and 48% higher ultimate loads, respectively, compared to conventional counterparts.
- Experimental results reveal the complex stress and strain behaviours of masonry columns under axial compression. Both CM and GPM specimens exhibit increased axial stress and strain with increasing confinement. Lateral strain also increases with axial stress, particularly in geopolymer mortar specimens. These findings underscore the importance of considering material type, confinement, and strain response in structural design and analysis.
- Comparing the IS 1905-1987 and Cascardi et al. (2017) models for predicting confinement ratios, significant variation is observed. The Cascardi model demonstrates superior accuracy, with a lower average Pre/Exp ratio, standard deviation, coefficient of variation, and higher R^2 value. Therefore, the Cascardi et al. (2017) model is more suitable for predicting masonry specimen confinement behaviour under axial compression compared to the IS 1905-1987 model. Further analysis and verification are recommended to ensure the reliability and applicability of the Cascardi et al. (2017) model across a wider range of masonry materials and configurations.

References

[1] J.F.D. Dahmen, and J.A. Ochsendorfs, "Earth Masonry Structures: Arches, Vaults and Domes," *Modern Earth Buildings Materials, Engineering, Constructions and Applications Woodhead Publishing Series in Energy*, pp. 427–460, 2012. [CrossRef] [Google Scholar] [Publisher Link]

[2] P.D. Gkournelos, T.C. Triantafillou, and D.A. Bournas, "Seismic Upgrading of Existing Masonry Structures: A State-of-the-Art Review," *Soil Dynamics and Earthquake Engineering*, vol. 161, 2022. [CrossRef] [Google Scholar] [Publisher Link]

[3] Valerio Alecci, Silvia Briccoli Bati, and Giovanna Ranocchia, "Study of Brick Masonry Columns Confined with CFRP Composite," *Journal of Composites for Construction*, vol. 13, no. 3, pp. 179–187, 2009. [CrossRef] [Google Scholar] [Publisher Link]

[4] B. Kondraivendhan, and Bulu Pradhan, "Effect of Ferrocement Confinement on Behavior of Concrete," *Construction and Building Materials*, vol. 23, no. 3, pp. 1218–1222, 2009. [CrossRef] [Google Scholar] [Publisher Link]

[5] Sachin B. Kadam, Yogendra Singh, and Bing Li, "Strengthening of Unreinforced Masonry Using Welded Wire Mesh and Micro-Concrete - Behaviour Under in-Plane Action," *Construction and Building Materials*, vol. 54, pp. 247–257, 2014. [CrossRef] [Google Scholar] [Publisher Link]

[6] Joseph Davidovits, and G. Resins, "Geopolymer Chemistry and Sustainable Development. The Poly (sialate) Terminology: A Very Useful and Simple Model for Thepromotion and Understanding of Green-Chemistry," *Geopolymer Green Chemistry and Sustainable Development Solutions, Geopolymer 2005 Conference*, Saint-Quentin, France, 2005. [Google Scholar]

[7] Joseph Davidovits, "*Geopolymer Cement a Review*," Geopolymer Science and Technics, Technical Paper #21, 2013. [Google Scholar] [Publisher Link]

[8] Waltraud M. Kriven, "Geopolymer-Based Composites," *Reference Module in Materials Science and Materials Engineering Comprehensive Composite Materials II*, vol. 5, pp. 269–280, 2018. [CrossRef] [Google Scholar] [Publisher Link]

[9] Behzad Majidi, "Geopolymer Technology, From Fundamentals to Advanced Applications: A Review," *Materials Technology*, vol. 24, no. 2, pp. 79–87, 2009. [CrossRef] [Google Scholar] [Publisher Link]

[10] Malathy Ramalingam et al., "Flexural Performance and Microstructural Studies of Trough-Shaped Geopolymer Ferrocement Panels," *Materials*, vol. 15, no. 16, pp. 1–19, 2022. [CrossRef] [Google Scholar] [Publisher Link]

[11] Taha Awadallah El-Sayed, "Axial Compression Behavior of Ferrocement Geopolymer HSC Columns," *Polymers*, vol. 13, no. 21, pp. 1-31, 2021. [CrossRef] [Google Scholar] [Publisher Link]

[12] S.S. Sneha et al., "Study of the Mechanical and Corrosion Resistance Properties of Ferrocement," *IOP Conference Series: Earth and Environmental Science*, vol. 491, no. 1, pp. 1–7, 2020. [CrossRef] [Google Scholar] [Publisher Link]

[13] Joseph Davidovits, "Properties of Geopolymer Cements," *First International Conference on Alkaline Cements and Concretes*, pp. 131–149, 1994. [Google Scholar] [Publisher Link]

[14] Mohana Rajendran, and Nagan Soundarapandian, "An Experimental Investigation on the Flexural Behavior of Geopolymer Ferrocement Slabs," *Journal of Engineering & Technology*, vol. 3, no. 2, 2013. [CrossRef] [Google Scholar] [Publisher Link]

[15] Mohana Rajendran, and Nagan Soundarapandian, "Behaviour of Geopolymer Ferrocement Slabs Subjected to Impact," *Iranian Journal of Science and Technology. Transactions of Civil Engineering*, vol. 38, no. C1+, pp. 223–233, 2014. [Google Scholar] [Publisher Link]

[16] Mohana Rajendran, and Nagan Soundarapandian, "Geopolymer Ferrocement Panels Under Flexural Loading," *Science and Engineering of Composite Materials*, vol. 22, no. 3, pp. 331–341, 2015. [CrossRef] [Google Scholar] [Publisher Link]

[17] Shaikh Mehedi Hasan, Shekh Muhsen Uddin Ahmed, and Waliul Islam "*Strengthening of Brick Masonry Column Using Ferrocement and Reinforced Concrete Jacketing*," Thesis, Bachelor of Science in Civil Engineering, Dhaka University of Engineering & Technology, Gazipur, 2018

[18] Debasish Sen et al., "Lateral Strength Evaluation of Ferrocement Strengthened Masonry Infilled RC Frame Based on Experimentally Observed Failure Mechanisms," *Structures*, vol. 58, 2023, [CrossRef] [Google Scholar] [Publisher Link]

[19] Andrei M. Reinhorn, S.P. Prawel, and Zi-He Jia, "Experimental Study of Ferrocement as a Seismic Retrofit Material for Masonry Walls," *Journal of Ferrocement*, vol. 15, no. 3, pp. 247–260, 1985. [Google Scholar]

[20] Ciro Faella et al., "Masonry Columns Confined by Composite Materials: Design Formulae," *Composites Part B: Engineering*, vol. 42, no. 4, pp. 705–716, 2011. [CrossRef] [Google Scholar] [Publisher Link]

[21] Eurocode 6 - EN1996-1-1, Design of Masonry Structures - Part 1-1: General Rules for Reinforced and Unreinforced Masonry Structures, CEN (European Committee for Standardization), 2005. [Online]. Available: https://www.phd.eng.br/wp-content/uploads/2015/02/en.1996.1.1.2005.pdf

[22] Indian Standards, IS 1905-1987: Code of Practice for Structural Use of Unreinforced Masonry, 3rd Revision, New Delhi, India, 1987. [Online]. Available: https://2cl405uvd.wordpress.com/wp-content/uploads/2015/06/is-1905-1987.pdf

[23] Alessio Cascardi et al., "Compressive Strength of Confined Column with Fiber Reinforced Mortar (FRM): New Design-Oriented-Models," *Construction and Building Materials*, vol. 156, pp. 387–401, 2017. [CrossRef] [Google Scholar] [Publisher Link]

[24] IS 1077 : 1992, Building Common Burnt Clay Building Bricks- Specifications, Indian Standard, 1992. [Online]. Available: https://law.resource.org/pub/in/bis/S03/is.1077.1992.pdf

[25] IS 4031-6: Methods of physical tests for hydraulic cement, Part 6: Determination of compressive strength of hydraulic cement (other than masonry cement), Bureau of Indian Standards, 1988. [Online]. Available: https://archive.org/details/gov.in.is.4031.6.1988/is.4031.6.1988/

[26] ASTM A 185-79, Standard Specification for Welded Steel Wire Fabric for Concrete Reinforcement, 1979. [Online]. Available: http://www.kleinreinforcing.com/filehandler.ashx?x=7942